Vibrational Spectroscopy 53 (2010) 296–306

Contents lists available at ScienceDirect

Vibrational Spectroscopy

journal homepage: www.elsevier.com/locate/vibspec

A combined DFT and vibrational spectroscopy study of the nickel and zinc O,O-diethyldithiophosphate complexes

Ferenc Billes[a,c,*], Allan Holmgren[b], Hans Mikosch[c]

[a] Department of Physical Chemistry and Material Science, Budapest University of Technology and Economics, H-1025 Budapest, Budafoki út 8, Hungary
[b] Division of Chemical Engineering, Department of Chemical Engineering and Geosciences, Luleå University of Technology, S-97187 Luleå, Porsön, Sweden
[c] Institute for Chemical Technologies and Analytics, Vienna University of Technology, A-1060 Wien, Getreidemarkt 9/164/EC, Austria

ARTICLE INFO

Article history:
Received 28 August 2008
Received in revised form 8 April 2010
Accepted 23 April 2010

Keywords:
Zinc and nickel complexes
FTIR
NIR FT Raman
Quantum chemistry
Normal coordinate analysis

ABSTRACT

Based on our earlier results on the theoretical and experimental study of potassium O,O-diethyldithiophosphate, the normal modes of nickel and zinc O,O-diethyldithiophoshate complexes were elucidated. Infrared and Raman spectra of these compounds were recorded. Quantum chemical calculations resulted in optimized structures, electric charge distributions, vibrational force constants, and fundamental frequencies. Normal coordinate analysis was applied to characterize the vibrational modes. Based on the results of these calculations vibrational spectra were simulated. The largest spectral differences between the two complexes appeared in vibrational modes encompassing the central part of the formula unit *viz.* PS_2MS_2P, where M is the metal atom. Namely, this central part of the Ni complex has D_{2h} symmetry, while that of the Zn one has D_{2d} symmetry.

1. Introduction

Dialkylthiophosphates (DADTPs) constitute an important group of collector molecules widely used in the separation and concentration of sulfide minerals [1]. Making the valuable mineral surfaces hydrophobic facilitates the flotation operation. However, dithiophosphates have also a number of other applications. In the metal–ligand complex with zinc DADTPs have for years been used as the most common and the best antiwear and antioxidant additive in engine and industrial oil formulations [2,3]. DADTPs have also been used as one of the starting chemicals in pesticide formulations, where the organic phosphate has the role of attacking the nervous system of insects, but for example Nickel DEDTP (E for ethyl) has also been applied as analytical reagent for spectrophotometric determination of transition metals [4,5].

To better understand the interaction between the metal atom and DEDTP in Ni and Zn complexes and especially the influence of the metal atom on the vibration frequencies of DEDTP, the combination of DFT calculations and experimental spectroscopic data seems to be a promising approach. This approach may also serve as an aid to the interpretation of vibrational spectra of DEDTP adsorbed at mineral surfaces containing NiS or ZnS. However, the combination of DFT and vibrational spectroscopy is very scant in the literature. Jiang et al. [6] studied the adsorption of diethyl, diisopropyl, diisobutyl and diphenyl esters of the dithiophosphate anion onto an α-Fe_2O_3 surface utilizing the ab initio HF method. Räsänen et al. [7] studied the methyl esters applying the MP2 method and the 6-31G* basis set, but examined only the molecular geometry and the charge distribution. Hellström et al. [8,9] and Fredriksson et al. [10] have utilized ab initio DFT methods in combination with ATR-FTIR spectroscopy to examine the vibrational properties of potassium heptyl xanthate both as a free molecule and as adsorbed on a Ge surface.

However, experimental vibrational spectroscopy of DEDTP combined with quantum chemical calculation is missing in the literature with the exception of Ref. [1]. In our previous work [11], the vibrational spectroscopy of potassium O,O′-diethyldithiophosphate (KDEDTP) was investigated by measuring the infrared and Raman spectra of the solid compound and simulating the spectra of the isolated molecule by fitting the calculated frequencies and intensities to the recorded spectra. The present work is an attempt to calculate the vibrational spectra of relatively large molecules *viz.* the complexes of Ni and Zn with KDEDTP. As an intermediate result of the quantum chemical calculations the optimized molecular geometric parameters were obtained. Vibrational spectra of the adsorbed collector were recorded applying the ATR method [12–14].

* Corresponding author at: Department of Physical Chemistry and Material Science, Budapest University of Technology and Economics, H-1521 Budapest, Budafoki út 8, Hungary. Tel.: +36 1 463 1267; fax: +36 1 463 3767.
E-mail address: fbilles@mail.bme.hu (F. Billes).

0924-2031/$ – see front matter © 2010 Elsevier B.V. All rights reserved.
doi:10.1016/j.vibspec.2010.04.011

2. Experimental

The nickel and zinc DEDPT compounds were prepared from the potassium salt of O,O′-diethyldithiophosphoric acid and $NiCl_2$ and $ZnCl_2$, respectively. The potassium salt was provided by CHEMINOVA. It is the major component of the commercial collector applied in sulfide ores flotation.

Infrared spectra were recorded using a Bruker IFS v/S spectrometer equipped with a DTGS detector and a diffuse reflectance accessory. The sample was diluted to 4% by weight in oven-dried spectroscopic grade potassium bromide and 200 scans were collected at 4 cm^{-1} resolution. The DRIFT spectra were transformed to Kubelka–Munk units.

Raman spectra were recorded using a Perkin Elmer NIR FT Raman 1700X spectrometer. The scattering was excited with intensity-stabilized 1064 nm emission from a Spectron SL 301 Nd:YAG laser, and the scattered light collected with a 180° backscattering-geometry lens. The laser power was 400 mW and 64 accumulations at 4 cm^{-1} resolution were detected by an indium gallium arsenide detector.

3. Calculations

For the quantum chemical calculations the Gaussian 03 program package [15] was used. The applied DFT functional was Becke3LYP [16,17]. The 6-311++G(df,p) basis set was used considering the nickel, zinc, phosphorus and the sulfur atoms.

The first step of the calculations was the optimization of the molecular structure. This step gave in addition to the optimized geometry (parameters and Cartesian coordinates) also the atomic net and NBO charges. During the second step the molecular energy function was differentiated twice with respect to the Cartesian coordinates. This step gave vibrational force constants, normal frequencies, atomic amplitudes in the normal modes, and molecular dipole moments.

The next step was the fit of the calculated entries to the experimental frequencies. At first the Cartesian coordinates were transformed to internal coordinates. The calculated force constants were also transformed into the new coordinate system. This natural internal coordinate system was chosen according to [18]. Performing the normal coordinate analysis the force constants were fitted to the experimental normal frequencies. For this fit identical scale factors were used for the force constants of the chemically similar coordinates. Subsequently, the potential energy distribution was calculated to describe the normal modes. The programs for all the calculations involved in this step were home-made ones.

In order to compare the experimental spectra with the calculated frequencies, infrared and Raman spectra were simulated using Lorentzian type bands with 15 cm^{-1} FWHH. This simulation is merely to get the frequency lines obtained from the calculations to appear like a real spectrum and should of course not be mixed up with an advanced simulation of the real line shapes. For the elaboration of the quantum chemical results our home-made programs were applied.

4. Results and discussion

The presented work is a possible model for the interaction between transition metal ions (like Ni and Zn) and dialkyldithiophosphates.

4.1. Molecular structures

The optimized molecular structures of the Ni and Zn DEDTP derivatives are shown in Fig. 1, where Fig. 1a1 shows the Ni(DEDTP)$_2$ complex and Fig. 1b1 the Zn(DEDTP)$_2$ complex in general view. Fig. 1a2 and a3 present two projections of Fig. 1a1, while Fig. 1b2 and b3 are similarly two projections of Fig. 1b1. Apparently, the PS_2MS_2P structures of the two complexes are quite different. As it can be seen, the space around the Ni atom is planar, whilst the structure around the Zn atom is tetrahedral, the two S_2M planes are perpendicular to each other.

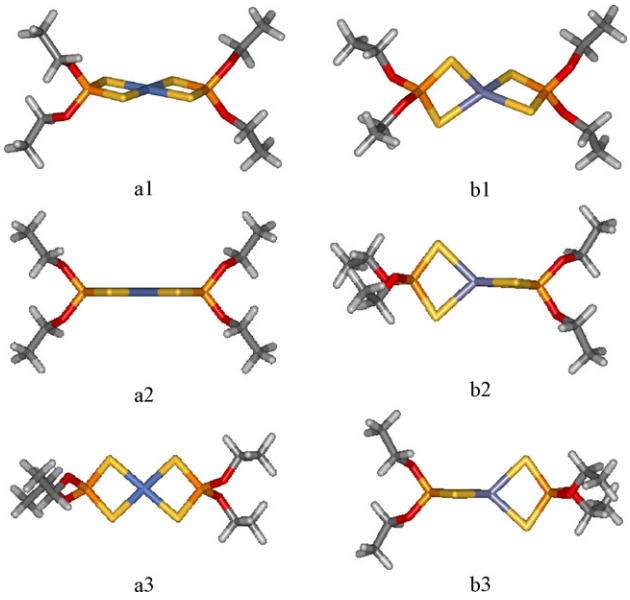

Fig. 1. Optimized structures of *a*: Ni(DEDTP)$_2$ and *b*: Zn(DEDTP)$_2$; a1, b1 are general views, a2 is the projection of the general view to the PS_2NiS_2P plane; a3 it its projection to the plane perpendicular to the PS_2NiS_2P plane; b2 is the projection of the general view to the PS_2Zn plane; b3 is its projection to the ZnS_2P plane.

The reason for this structural difference must be the difference in the electronic structures of the two atoms. The electronic ground state of the Ni atom is $Ar3d^84s^2$, whilst the electronic structure of the Zn atom is $Ar3d^{10}s^2$. During the complex formation each of the four sulfur atoms donate two electrons to the Ni^{2+} ion ($Ar3d^8$) saturating its 3d subshell to d^{10}, two electrons build the 4s subshell, the remaining four ones occupy 4p orbitals. The resulting Ni structure in its complex is $Ar3d^{10}4s^2p^4$ corresponds the dsp^2 hybrid and implying therefore the observed planar structure. According to Fig. 1a2 and a3 and the dsp^2 hybridization and the central part of the complex (PS_2NiS_2P) has three mutually perpendicular twofold rotational axes crossing each other in the Ni atom, and three mutually perpendicular symmetry planes. Therefore the central part has D_{2h} symmetry.

The Zn^{2+} ion (Ard^{10}) is donated on similar way by the four sulfur atoms and the Zn electron structure in the formed Zn(DEDTP)$_2$ complex is $Ar3d^{10}4s^2p^6$. This sp^3 hybrid structure should have to form a tetrahedral space around it. However, the four sulfur atoms are symmetrically not equivalent. They belong by pairs (S4, S5 and S24, S25, respectively) to their own DEDTP groups (see Fig. 2). Therefore the expected T_d symmetry around the Zn atom is distorted, the PS_2ZnS_2P central group stretches along the P–Zn–P line. So this group has a fourfold rotation–reflection symmetry axis (the P–Zn–P line), two symmetry planes, each of them contains one of the ZnS_2P rings and intersect in the P–Zn–P line, and twofold rotational symmetry axes in the bisectors of the symmetry planes, perpendicular to each other and also the rotation–reflection axis. These symmetry elements correspond to D_{2d} symmetry.

That is, the central parts of these compounds have relatively high symmetry. Table 1 shows the molecular parameters of the compounds. Regarding to their symmetry, only half of the bond lengths and valence angles are shown, with the exclusion of those

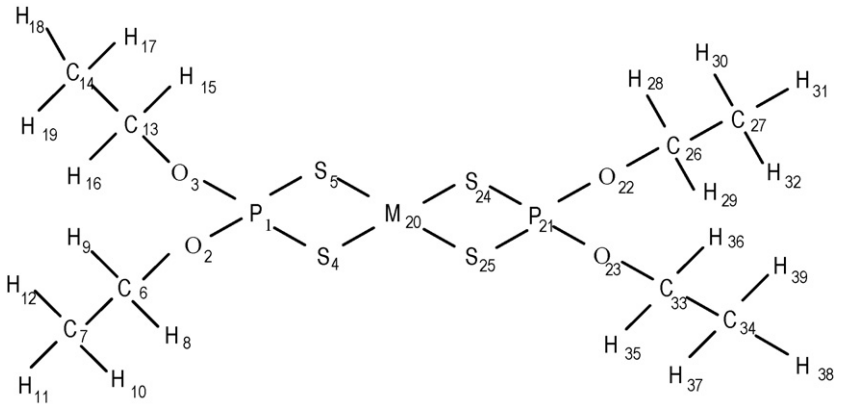

Fig. 2. Numbering of the atoms of the investigated molecules; M: metal, Ni or Zn.

bonds belonging to the metal atom. The table lists also two torsional angles demonstrating the structure of the central groups. The same parameters for the ionic KDEDTP salt are included for comparison. For this purpose the properties of the potassium salt molecule were recalculated with Becke3LYP functional and the 6-311++G(df,p) basis set (see Ref. [11]). Fig. 2 gives the numbering of the atoms.

According to Table 1, the structure around the Zn and Ni atoms in the PS_2MS_2P part of the molecules exhibits large differences. The difference in the S–Ni and S–Zn bond lengths reflect the different structures of the central groups. Of course the potassium ion has an even longer distance to the sulfur atom because this interaction is ionic and therefore not covalent in its character. Large differences are also observed for the valence angles with vertex at the metal atom and in the torsional angles around the M–P line. This reflects the structural differences in the center of the molecules. Compare, for example, the values of the τ(P21, M20, P1, O2) and the τ(P21, M20, P1, O3) torsional angles of the Ni and the Zn complexes. They reflect the differences in the symmetries of the central parts of molecules.

Table 1
Selected geometric parameters of the studied O,O-diethyldithiophosphates[a].

Parameter[b,c]	Ni	Zn	K[d]
r(P1,M20)	2.844	2.909	3.466
r(P21,M20)	2.844	2.909	
r(P1,O2)	1.605	1.603	1.625
r(P1,O3)	1.605	1.604	1.625
r(P21,O22)	1.605	1.604	
r(P21,O23)	1.605	1.603	
r(P1,S4)	2.007	2.022	2.010
r(P1,S5)	2.007	2.024	2.010
r(P21,S24)	2.007	2.024	
r(P21,S25)	2.007	2.003	
r(O2,C6)	1.451	1.452	1.441
r(O3,C13)	1.451	1.452	1.441
r(S4,M20)	2.274	2.427	2.997
r(S5,M20)	2.274	2.422	2.997
r(S24,M20)	2.274	2.428	
r(S25,M20)	2.274	2.421	
φ(O2,P1,O3)	103.9	104.7	103.3
φ(S4,P1,S5)	105.1	110.8	119.0
φ(O2,P1,S4)	108.8	107.2	111.4
φ(S4,M20,S5)	88.9	86.8	70.6
φ(O3,P1,S5)	108.8	107.1	111.4
φ(O2,P1,S5)	115.3	113.6	105.3
φ(O3,P1,S4)	115.3	113.4	105.3
φ(O2,P1,M20)	128.2	129.8	128.3
φ(O3,P1,M20)	127.9	125.6	128.3
φ(P1,O2,C6)	121.4	121.3	122.1
φ(P1,O3,C13)	121.4	121.4	122.1
φ(O2,C6,C7)	107.8	107.7	107.9
φ(O3,C13,C14)	107.9	107.8	107.9
φ(O2,C6,H8)	108.3	108.5	109.0
φ(O3,C13,H15)	108.3	108.3	109.0
φ(O2,C6,H9)	109.0	108.7	109.1
φ(O3,C13,H16)	109.0	108.9	109.1
τ(P1,M20,P21,O22)	−176.30	−135.70	
τ(P1,M20,P21,O23)	3.70	45.20	

[a] Distances in Å, angles in°.
[b] r: bond lengths; φ: valence angles; τ: torsion angles; M: metal.
[c] For the structures see Fig. 1, for the numbering the atoms see Fig. 2.
[d] Ref. [11].

4.2. Atomic net charges

Both Mulliken's atomic net charges [19] and the natural NBO/NPA atomic charges [20,21] were calculated. The results are listed in Table 2. Regarding the molecular symmetries only the charges of 20 atoms are listed for each molecule.

The comparison between Mulliken's net charges and the atomic natural ones is not an easy task since the theoretical background of the two methods was very different. Looking at the results there are surprising differences between the Mulliken's and the NBO charges. All of the NBO charges have the same sign for P and O, respectively, whilst the Mulliken's values for the phosphorus and oxygen atoms of the K salt are opposite in sign as compared to these values for the Zn and Ni complexes.

The definition of Mulliken's charges is based on population analysis. The *Mulliken population analysis* provides a partitioning of either the total charge density or an orbital density. The number of the electrons in the molecule (N) is the integral of the charge density over the space. N is partitioned for all atoms considering also the overlap population. According to the theory the overlap population of atoms A and B is divided between the two atoms in half-to-half ratio. This is one weak point of the theory. The other weak point is its strong dependence on the basis set applied. Our Mulliken's atomic net charges are comparable since the same basis set was used for the Ni and Zn compounds as well as for the K salt. The atomic net charge is the difference between the calculated number of electrons belonging to the atom in the complex/salt and the number of electrons of the isolated atom.

The natural atomic charge is based on the theory of the *natural population analysis*. The analysis is carried out with natural bond orbitals (NBO). They are linear combinations of the natural atomic orbitals. The derivation of a valence-shell atomic orbital (NAO) involves diagonalization of the localized block of the full density matrix of a given molecule associated with basis functions on that atom. A distinguishing feature of NAOs is that they meet the simultaneous requirement of orthonormality and maximum occupancy. In a polyatomic molecule the NAOs mostly retain one-center character, and thus they are optimal for describing the molecular

Table 2
Atomic net charges of O,O-diethyldithiophosphates[a,b].

Serial number[c]	Atom type	Ni complex		Zn complex		K salt	
		Mulliken	NBO	Mulliken	NBO	Mulliken	NBO
1	P	0.648	1.675	0.604	1.673	-0.662	1.618
2	O	−0.381	−0.850	−0.380	−0.849	0.153	−0.873
4	S	−0.421	−0.557	−0.534	−0.700	−0.220	−0.750
6	C	−0.094	−0.013	−0.091	−0.013	−0.216	−0.026
7	C	−0.374	−0.582	−0.374	−0.582	−0.526	−0.585
8	H	0.174	0.182	0.179	0.184	0.127	0.187
9	H	0.149	0.169	0.148	0.168	0.186	0.165
10	H	0.153	0.206	0.154	0.206	0.168	0.204
11	H	0.142	0.199	0.145	0.201	0.152	0.201
12	H	0.136	0.204	0.136	0.204	0.163	0.202
20	M	0.767	0.814	1.274	1.385	0.686	0.932

[a] Atomic net charges in atomic charge units; M: metal.
[b] Data of only one of the symmetrically equivalent atoms are presented.
[c] For the numbering of the atoms see Fig. 2.

electron density around each atomic center. Natural bond orbitals are linear combinations of the NAOs of two bonded atoms. The natural population analysis satisfies Pauli's exclusion principle and solves the basis set dependence problem of the Mulliken's population analysis.

Concerning the metal atom charges, both methods find the Zn atom more positive than the Ni atom, the difference being 0.5–0.6 atomic charge units (a.ch.u.). According to the theory of NBOs, the charge difference does not act farther than to the next sulfur atom. Near the more positively charged Zn atom, the S atoms are more negatively charged than those around the Ni atom. On the contrary, according to Mulliken, this additional positive charge of Zn propagates up to the phosphorus atom (see Figs. 1 and 2 for the position of the atoms in the molecules).

Both Mulliken and NBO charges of the P atoms are positive for the Ni and Zn complexes. However, according to Mulliken, the phosphorus atoms are less positively charged than the metal atoms in the two complexes, whilst the NBO charges show that the phosphorus atoms are more positively charged. However, both methods find the oxygen atoms to be negatively charged.

At a longer distance from the metal ion, the carbon atoms of the ethyl groups have only small negative charges.

There is clearly an important difference between the K salt and the covalent Ni or Zn DEDTP complexes as evident from the very different charge distributions of the formula units and this was the reason for including charges of the K salt in Table 2.

4.3. Vibrational force constants

The vibrational force constants can tell something about the interatomic forces of the molecule. However, it is a challenge to extract this information since the molecules in question with their 39 atoms have 1 1 1 vibrational modes and accordingly the force constant matrices have $1\,1\,1 \times 1\,1\,1$ elements. Of course, the full force constant matrix was applied in the GF matrix eigenvector–eigenvalue calculations. For practical use, only the diagonal elements are presented (see the supplementary Table S1 in Appendix A in the online version).

Table S1 describes the definition of the applied (1 1 1) internal coordinates, the optimized scale factors applied for the fitting of the quantum chemical (QCH) force constants to the experimental frequencies, and the diagonal scaled (SC) force constants (for the SC frequencies see Tables 3 and 4). The same internal coordinate set and scale factor set was used for the Ni and the Zn complexes.

As already indicated in the Calculation section above, we used the normal *internal coordinate* set [18]. The coordinate system was constructed radially. At first the coordinates of the central PS_2MS_2P group were defined (coordinates 1–15), the 8 stretchings (S–M and S–P ones), 3 in-plane deformations and 4 torsion coordinates. The next 12 coordinates describe the joining of the four oxygen atoms (2, 3, 22 and 23) to the central group with one–one stretching, in-plane deformation and out-of plane deformation coordinates, respectively. Each ethyl group needs 21 coordinates, coordinates 28–48, 49–69, 70–90 and 91–111, respectively.

Altogether only 16 different *scale factors* were used for the scaling of the 1 1 1 vibrational modes. The scale factors for the torsional coordinates 8 and 9 are extremely high. These coordinates belong to the turnings of the S_2MS_2 group. Since these groups are rather rigid, their turnings lead to non-linear motions, i.e. a non-linear motion is described in the frame of a linear approach. This is the reason of the high scale factors of 1.560. The values of all other scale factors are between 0.777 and 1.095.

The vibrational force constants of the symmetrically equivalent internal coordinates show small deviations (see e.g. their values for the 1, 2, 3, and four coordinates). The reason of these deviations is the systematic error of the second derivation in the quantum chemical calculations.

Comparing the force constants of the nickel and zinc complexes some interesting deviations can be observed. Paying attention to the *central groups* of the molecules the S–M stretching force constants of the Ni and the Zn complexes have very close values (internal coordinates 1–4), the deviations are about 10%. Looking at the P–S force constants (internal coordinates 10–13) the differences are only about 2.5%. However, the deformation force constants (in-plane deformations, 5–7, SSMS torsions, 8–9) reflect very nice the differences in the structures (Table 1) of the central group symmetries. There are great deviations and also changes in the order of the force constant values. The values of the SSMS torsions (internal coordinates 14–15) are very low in comparison with the SSMS ones. The changes in their order can also be seen here.

The force constants of the O–P stretchings (16–19) are very close with about 1% to the benefit of the Zn complex. For the corresponding deformation force constants (in-plane 20–23, out-of-plane 24–27) the values for the Zn complex are about 12–15% higher.

The force constants reflecting the internal forces in the ethyl groups show in almost all cases only negligible differences between the corresponding values for the Ni and Zn complexes.

4.4. Characterization of the vibrational modes

The SC vibrational frequencies of the molecules can be computed from the eigenvalues of the *GF* matrix (inverse kinetic energy matrix × force constant matrix). The elements of the potential energy matrix (PED) were calculated from the eigenvector matrix

Table 3
Measured and calculated (scaled) vibrational frequencies (cm^{-1}) of nickel O,O-dimethyldithiophosphate.

Frequencies[a]		Potential energy distributions Type[b] % (only not less then 10)			
Measured	Calculated				
2988.6	2989.2	ν CH 99			
2988.6	2989.2	ν CH 99			
2988.6	2988.8	ν CH 99			
2988.6	2988.8	ν CH 99			
2979.0	2977.3	ν CH 99			
2979.0	2977.2	ν CH 99			
2979.0	2977.2	ν CH 99			
2979.0	2977.2	ν CH 99			
2937.6	2948.3	ν CH 99			
2937.6	2948.3	ν CH 99			
2937.6	2947.7	ν CH 99			
2937.6	2947.7	ν CH 99			
2923.6	2913.5	ν CH 99			
2923.6	2913.4	ν CH 99			
2923.6	2913.3	ν CH 99			
2923.6	2913.3	ν CH 99			
2900.7	2907.7	ν CH 99			
2900.7	2907.6	ν CH 99			
2900.7	2907.5	ν CH 99			
2900.7	2907.5	ν CH 99			
1473.3	1474.1	ν CH 99			
1473.3	1474.1	β CH 84			
1473.3	1474.0	β CH 93			
1473.3	1473.9	β CH 93			
1454.2	1453.4	β CH 98			
1454.2	1453.1	β CH 98			
1454.2	1452.7	β CH 99			
1454.2	1452.5	β CH 99			
1443.5	1444.2	β OCH 92			
1443.5	1444.0	β OCH 92			
1443.5	1439.7	β OCH 92			
1440.2	1439.7	β OCH 92			
1400.0	1400.8	β CH 83			
1400.0	1400.7	β CH 83			
1400.0	1398.4	β CH 82			
1400.0	1398.3	β CH 82			
1388.9	1376.9	β CH 97			
1388.9	1376.9	β CH 97			
1388.9	1375.8	β CH 97			
1388.9	1375.7	β CH 97			
1284.7	1282.9	β CH 98			
1284.7	1282.6	β CH 98			
1284.7	1282.0	β CH 97			
1288.7	1281.8	β CH 97			
1157.6	1156.6	β CH 99			
1157.6	1156.1	β CH 99			
1157.6	1156.1	β CH 99			
1157.0	1155.6	β CH 99			
1105.2	1107.3	β CH 50	ν CC 29		β CCO 15
1105.2	1107.3	β CH 50	ν CC 28		β CCO 15
1105.2	1104.9	β CH 51	ν CC 29		β CCO 15
1105.2	1104.9	β CH 15	β CH 36	ν CC 29	β CCO 15
1047.5	1030.3	ν PO 29	ν CO 43	ν CC 18	
1005.9	1019.3	ν PO 19	ν CO 40	ν CC 26	
1005.9	1012.5	ν PO 19	ν CO 37	ν CC 25	
1005.9	1012.0	ν PO 18	ν CO 37	ν CC 26	
970.3	973.5	ν PO 46	ν CC 31		
970.3	972.9	ν PO 46	ν CC 31		
970.3	971.9	ν PO 35	β CH 20		ν CC 39
970.3	966.3	ν PO 43	ν CC 32		
808.3	807.7	β CH 95			
808.3	807.4	β CH 98			
808.3	806.6	β CH 98			
808.3	806.3	β CH 97			
808.3	785.1	ν PO 28	ν CO 35	β CH 11	
779.6	784.7	ν PO 27	ν CO 37	β CH 11	
779.6	768.3	ν PO 27	ν CO 35		
779.6	766.8	ν PO 30	ν CO 32	β CH 10	
644.2	639.7	ν SP 61	δ OSP 18		
636.3	628.5	ν SP 65	δ OSP 18		
548.0	554.1	ν SP 50	δ OSP 17	β CCO 11	
548.0	550.6	ν SP 51	δ OSP 17	β CCO 11	

Table 3 (*Continued*)

Frequencies[a]		Potential energy distributions Type[b] % (only not less then 10)			
Measured	Calculated				
404.2	414.1	β OPS 27	β CCO 38		
404.2	413.0	β OPS 26	β COP 10	β CCO 39	
404.2	397.8	ν SP 21	δ OSP 39	ν CO 10	
404.2	391.9	ν SP 22	δ OSP 39	ν CO 10	
347.5	339.8	δ OSP 42	ν CO 11	β CCO 10	
333.3	332.0	δ OSP 44	ν CO 11	β CCO 10	
333.3	326.8	δ OSP 14	β CCO 44		
333.3	326.8	δ OSP 15	β CCO 48		
305.8	297.2	ν NiS 77	β SNiS 18		
305.8	285.2	ν NiS 83	β SNiS 10		
244.6	257.3	τ SSNi 17	β OPS 45		
244.6	257.1	ν NiS 57	β OPS 16	τ HCC 11	
244.6	249.3	β OPS 27	β COP 21	τ HCC 27	
244.6	244.9	ν NiS 34	β OPS 12	β COP 21	τ HCC 13
244.6	244.6	β OPS 36	τ HCC 37		
244.6	233.6	τ HCC 79			
220.8	223.2	β OPS 42	τ HCC 27		
220.8	221.2	β OPS 19	β COP 12	τ HCC 59	
220.8	220.6	β OPS 20	τ HCC 62		
220.8	208.2	ν NiS 90			
177.4	183.5	ν NiS 17	ν SP 10	β SNiS 52	
177.4	177.4	τ SSNi 47	β OPS 30		
128.3	129.8	β SNiS 36	δ OSP 11	β COP 37	
128.3	117.5	β SNiS 76			
101.0	108.7	τ SSNi 28	β OSP 12	δ OSP 13	β COP 34
98.5	97.9	δ OSP 29	β COP 38		
98.5	93.1	β OPS 20	δ OSP 21	β COP 43	
76.5	76.4	β SNiS 14	δ OSP 12	β COP 11	τ COP 35
62.0	61.3	τ COP 65	τ CCO 20		
52.6	51.8	τ COP 74	τ CCO 14		
51.1	50.7	τ COP 65	τ CCO 22		
45.3	45.5	β SNiS 22	δ OSP 15	τ COP 26	
44.6	44.7	τ COP 20	τ CCO 76		
44.6	44.7	τ COP 19	τ CCO 76		
34.2	34.4	τ COP 13	τ CCO 79		
32.5	32.9	τ SSNi 56	δ OSP 10	β COP 12	
32.5	32.6	β OPS 10	τ COP 17	τ CCO 61	
9.8	11.3	τ PSNi 77			
9.8	11.0	τ PSNi 75			

[a] Mean deviation 4.75 cm^{-1}; mean relative deviation 1.23%.
[b] ν: stretching; β: in-plane-deformation; δ: out-of-plane deformation; τ: torsion.

of *GF*. Tables 3 and 4 show the experimental and SC fundamental frequencies of Ni DEDTP and Zn DEDPT, respectively. Here the PED elements are listed, too. The contributions of the similar internal coordinate types are summarized.

For the scaling we preferred the experimental Raman spectra since their recorded region is extended to the lower frequency region ($\geq$200 cm^{-1}). The frequencies of vibrational modes including the metal atom appear in this region. Experimental frequencies below 200 cm^{-1} were substituted for calculated quantum chemical results. The overlapping bands were resolved.

The number of the experimental vibrational bands is less than the number of the vibrational modes calculated. Therefore we had to use multiple assignments. Sometimes the calculated SC frequencies are closer than the resolution of the experimental spectra. The experimental band at 1443.5 cm^{-1} was assigned to three calculated frequencies for the Ni DEDTP complex. Since the positions of the P–O-ethyl groups in the molecules are very close, the resolution of the calculated frequencies are sometimes less then 0.05 cm^{-1}. Therefore these frequencies appear in the tables as being identical (see Table 3).

With the exclusion of the CH stretching vibrations and several CH in-plane deformation vibrations all other movements of the atoms (internal coordinates) are distributed over many vibrational modes. Looking at these distributions one can conclude that the modes where the contribution to the intensity is due to many adjacent vibrational modes imply a broader spectral region. The P–S, M–S, P–O, C–O and C–C stretchings and deformations are similarly distributed over several vibrational modes. This is characteristic of the so-called finger print region of vibrational spectra where spectral interpretations may be very ambiguous without first making a normal coordinate analysis using a reliable method. The broadness of the bands may also be due to the conformation of the ethyl entities. A small change in the conformation may result in only a small increase in the total energy of the molecule and transitions between these local minima should contribute to the band shape. Now the distribution of the P–S and M–S stretching coordinates and also those of the P–O and C–O stretching will be discussed in more detail.

The P–S stretching motions are the 5th (P1–S4, left low), the 8th (P21–S25, right low), the 21st (P1–S5, left high), and the 30th (P21–S24, right high) internal coordinates (see Fig. 2). The P–S stretching motions in $Ni(DEDTP)_2$ are distributed above all over four vibrational modes (see Table 3) with SC frequencies 639.7 cm^{-1} (61%), 628.5 cm^{-1} (65%), 554.1 cm^{-1} (50%) and 550.6 cm^{-1} (51%). The first one is a vibration with the 11th and the 13th (the two lower) coordinates moving in phase, while the two other move in opposite phase. The second motion is a mode, where the two opposite coordinates (the 10th and the 13th) are in phase and the two other move anti-phase. In the third mode all the P–S coordinates move in phase. At last, in the fourth vibrational mode the two left (12th and 13th) coordinates are in phase, whilst the right ones move in opposite phase.

Table 4
Measured and calculated (scaled) frequencies (cm^{-1}) of zinc O,O-diethyldithiophosphate.

Frequencies[a]		Potential energy distributions			
Measured	Calculated	Type[b] % (only not less than 10)			
2982.0	2990.0	ν CH 99			
2982.0	2990.0	ν CH 99			
2982.0	2989.1	ν CH 99			
2982.0	2989.0	ν CH 99			
2964.3	2977.5	ν CH 99			
2964.3	2977.5	ν CH 99			
2964.3	2977.4	ν CH 99			
2964.3	2977.4	ν CH 99			
2938.9	2948.3	ν CH 99			
2938.9	2948.2	ν CH 99			
2938.9	2946.3	ν CH 99			
2938.9	2946.2	ν CH 99			
2927.5	2913.6	ν CH 99			
2927.5	2913.5	ν CH 99			
2927.5	2913.4	ν CH 99			
2927.5	2913.4	ν CH 99			
2895.8	2908.3	ν CH 99			
2895.8	2908.3	ν CH 99			
2895.8	2907.4	ν CH 99			
2895.8	2907.4	ν CH 99			
1471.5	1474.5	β CH 92			
1471.5	1474.4	β CH 92			
1471.5	1474.3	β CH 90			
1471.5	1474.3	β CH 98			
1452.2	1452.9	β CH 98			
1452.2	1452.2	β CH 99			
1452.2	1452.0	β CH 98			
1452.2	1451.3	β CH 99			
1440.6	1444.0	β OCH 91			
1440.6	1443.8	β OCH 91			
1440.6	1437.6	β OCH 92			
1440.6	1437.6	β OCH 92			
1390.8	1399.6	β CH 93			
1390.8	1399.6	β CH 92			
1390.8	1397.3	β CH 31	β CH 61		
1390.8	1397.2	β CH 61	β CH 31		
1364.7	1376.1	β CH 66	β CH 31		
1364.7	1376.1	β CH 31	β CH 66		
1364.7	1373.9	β CH 63	β CH 34		
1364.7	1373.9	β CH 34	β CH 63		
1276.0	1282.4	β CH 95			
1276.0	1282.2	β CH 95			
1276.0	1278.0	β CH 91			
1276.0	1277.9	β CH 91			
1160.2	1156.0	β CH 99			
1160.2	1155.5	β CH 99			
1160.2	1155.4	β CH 42	β CH 56		
1160.2	1155.0	β CH 11	β CH 87		
1105.7	1107.8	β CH 28	β CH 22	ν CC 29	β CCO 15
1105.7	1107.7	β CH 22	β CH 28	ν CC 29	β CCO 15
1105.7	1104.9	β CH 48	ν CC 29	β CCO 15	
1105.7	1104.9	β CH 48	ν CC 29	β CCO 15	
1011.4	1029.1	ν PO 29	ν CO 43	ν CC 17	
1011.4	1020.8	ν PO 22	ν CO 42	ν CC 23	
1011.4	1015.1	ν PO 26	ν CO 36	ν CC 19	
1011.4	1013.9	ν PO 24	ν CO 36	ν CC 20	
960.3	977.2	ν PO 40	β CH 10	ν CC 37	
960.3	976.9	ν PO 42	β CH 10	ν CC 36	
960.3	971.9	ν PO 36	β CH 10	β CH 10	ν CC 39
960.3	968.3	ν PO 41	ν CC 34		
813.8	804.4	β CH 97			
813.8	804.0	β CH 45	β CH 51		
813.8	803.6	β CH 97			
813.8	803.4	β CH 97			
775.5	786.6	ν PO 26	ν CO 37	β CH 11	β CH 10
775.5	785.9	ν PO 26	ν CO 38	β CH 10	β CH 11
775.5	764.7	ν PO 28	ν CO 36	β CH 10	
775.5	763.8	ν PO 30	ν CO 33	β CH 10	
613.9	619.7	ν SP 58	δ OSP 20		
613.9	617.0	ν SP 59	δ OSP 20		
541.0	543.9	ν SP 45	δ OSP 24	β CCO 11	
541.0	539.9	ν SP 45	δ OSP 23	β CCO 11	
419.1	410.2	β OPS 26	β CCO 38		
419.1	409.9	β OPS 25	β CCO 39		

Table 4 (*Continued*)

Frequencies[a]		Potential energy distributions			
Measured	Calculated	Type[b] % (only not less than 10)			
391.9	394.6	ν SP 33	δ OSP 30		
391.9	393.7	ν SP 33	δ OSP 29		
334.7	339.6	ν SP 10	δ OSP 45	β CCO 10	
334.7	339.5	δ OSP 40	ν CO 16		
313.6	316.7	δ OSP 18	β CCO 48		
313.6	316.2	δ OSP 18	β CCO 47		
295.8	265.3	ν ZnS 29	β OPS 26	τ HCC 18	
295.8	263.2	ν ZnS 13	β OPS 31	β COP 11	τ HCC 26
243.8	251.9	β OPS 49	τ HCC 16		
243.8	248.8	β OPS 46	τ HCC 20		
243.8	247.9	ν ZnS 57			
243.8	242.7	ν ZnS 68	β COP 12		
243.8	227.8	β OPS 25	τ HCC 51		
243.8	226.4	β OPS 32	τ HCC 41		
235.5	218.3	β OPS 19	β COP 11	τ HCC 55	
234.7	217.3	β OPS 23	τ HCC 62		
195.4	192.1	β SZnS 71			
191.6	169.4	ν ZnS 64	β COP 20		
191.5	167.7	ν ZnS 63	β COP 24		
107.8	110.9	τ SSZn 51	β COP 10		
107.5	105.5	β SZnS 40	τ SSZn 11	β COP 12	
106.8	100.5	ν ZnS 10	β SZnS 36	β COP 24	
105.8	98.1	δ OSP 23	β COP 24	τ COP 12	
101.4	93.8	β OPS 24	δ OSP 19	β COP 42	
93.4	86.8	β SZnS 35	δ OSP 16	τ COP 19	
84.9	78.5	τ SSZn 40	β COP 14	τ COP 26	
66.6	75.4	ν ZnS 12	δ OSP 16	τ COP 44	
62.9	57.7	β SZnS 26	τ COP 64		
58.9	54.1	β SZnS 19	τ COP 71		
58.7	53.3	τ COP 79			
38.8	36.1	τ CCO 81			
36.5	34.0	τ CCO 87			
30.4	28.9	τ SSZn 63	τ CCO 12		
29.3	28.3	τ CCO 91			
24.0	27.3	τ CCO 84			
14.8	14.1	τ PSZn 69	β OPS 11		
11.8	10.6	τ PSZn 71			

[a] Mean deviation: 7.07 cm^{-1}; mean relative deviation: 2.36%.
[b] ν: stretching; β: in-plane-deformation; δ: out-of-plane deformation; τ: torsion.

The P–S stretching coordinates in $Zn(DEDTP)_2$ show a similar distribution giving rise to four vibrational modes (see Table 4). These modes appear at somewhat lower frequencies *viz.* at 619.7 cm^{-1} (58%), 617.0 cm^{-1} (59%), 543.9 cm^{-1} (45%), and 539.9 cm^{-1} (45%). In the first of these modes, the two opposite coordinates (10th and 13th) move in phase, whereas the other two move opposite to them (out-of-phase). In the second one the two lower coordinates (11th and 13th) move in phase, whilst the two other vibrate anti-phase. The third one is a mode where all coordinates move in phase. Regarding the forth one, the two left coordinates (12th and 13th) vibrate in phase, the other ones move anti-phase.

According to the spectral interpretations, the basis of this analysis is that the first and second vibrational modes can be regarded as true P–S vibration since the participation of these coordinates describes the major part of the mode. The third and the fourth modes can be regarded as true P–S vibrations only for the Ni complex.

According to data in supplementary Table S1, four M–S internal stretching coordinates were defined, the first four, see also Fig. 2. These coordinates are also distributed over several vibrational modes, they are dominated above all in four vibrational modes, and are coupled like the P–S stretching vibrations.

For the SC frequencies of the Ni compound (see Table 3), the four modes with the highest Ni–S stretching participation are those at 297.2 cm^{-1} (77%), 285.2 cm^{-1} (83%) 257.1 cm^{-1} (57%) and 208.2 cm^{-1} (90%). In the first vibrational mode the two right stretchings (1st and 2nd) move in phase, the two other, namely the 3rd and the 4th in opposite one to them (see Fig. 2). Regarding the second mode, here the upper stretching coordinates (1st and 3rd) vibrate in phase, while the two other in opposite phase. In the third normal mode all stretchings move in phase. At last, in the fourth vibration two opposite coordinates (the 1st and the 4th) vibrate in phase, the two other in opposite phase to them.

In $Zn(DEDTP)_2$ the vibrational modes with Zn–S participation themselves were found at lower SC frequencies (see Table 4) then those of the Ni–S ones. The four SC frequencies with highest participations are at 247.9 cm^{-1} (57%), 242.7 cm^{-1} (68%), 169.4 cm^{-1} (64%), and 168.9 cm^{-1} (63%). In the first of them the right coordinates (1st and 2nd) vibrate in phase, the two other (3rd and 4th) in opposite phase to them (see Fig. 2). The second mode is the mode where all the stretching vibrate in phase. Regarding the third normal vibration, the upper coordinates (1st and 3rd) move in phase, the other in opposite phase. The fourth mode is that where the opposite internal coordinates (1st and 4th) vibrate in phase, the two other in opposite phase.

These results show that there exist four normal modes for both the nickel and the Zn complexes, respectively, where the participation of the M–S stretchings are over 50%, i.e. they can be regarded as true M–S stretching modes.

The distribution of the P–O stretching motion over the vibrational modes is similar in both $Ni(DEDTP)_2$ and $Zn(DEDTP)_2$ spectra. There are two spectral regions showing these coordinates participate in relevant amounts. In eight vibrational modes between 1030 cm^{-1} and 960 cm^{-1}, the contribution from P–O stretching amounts to 19–46% and four vibrational modes between 790 cm^{-1} and 760 cm^{-1} the contribution is 25–30% (Tables 3 and 4).

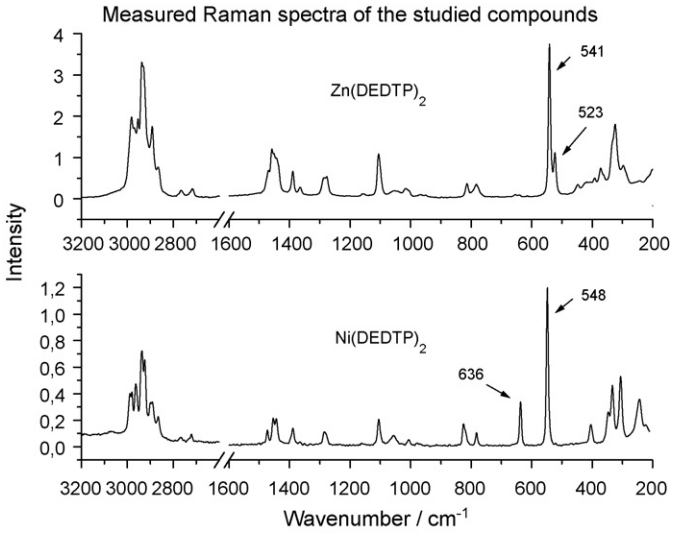

Fig. 3. Measured Raman spectra of the studied compounds.

4.5. Experimental and simulated vibrational spectra

The measured Raman and infrared spectra of $Ni(DEDTP)_2$ and $Zn(DEDTP)_2$ were compared with the calculated infrared and Raman spectra in order to assign some of the more prominent spectral changes.

Fig. 3 shows the measured Raman spectra of the two compounds. The line with the highest intensity is observed at 548 cm^{-1} in the spectrum of the $Ni(DEDTP)_2$ complex. This line corresponds to the absorption at 541 cm^{-1} in the $Zn(DEDTP)_2$ spectrum. According to the normal coordinate analysis, the P–S stretching coordinates dominate at these frequencies (see the previous section). This knowledge is of course important since the P–S entity of the two molecules is expected to take part in interactions with metal sulfide surfaces in the flotation process as well as with iron atoms in tribological applications.

The line of medium intensity in the Raman spectrum of the Ni compound at 636 cm^{-1} is missing in the Raman spectrum of the Zn compound. However, a line of medium intensity appeared in the Raman spectrum of the Zn complex at 523 cm^{-1}, a line that is missing in the spectrum of the Ni compound. Both of these lines have considerable P–S stretching content. This clear difference in the Raman spectra of the two compounds is not very surprising considering the sensitivity of the Raman technique to respond to structural changes. The ligands in the Ni complex are coordinated to the nickel atom in a planar configuration (Fig. 1), whilst the ligands in the Zn complex are coordinated to the Zn atom forming a tetrahedral structure (Fig. 2). In a previous investigation it was suggested that DEDTP forms a bridging binuclear coordination to Zn atoms at the surface of synthetic sphalerite [22]. However, in e.g. deuterated chloroform solution the originally polynuclear DEDTP Zn(II) complex in the solid state dissociates with a subsequent transition to a mononuclear state [23], which makes our assumption of a tetrahedral structure (Fig. 2) reasonable at least before the collector is adsorbed from aqueous solution onto a sphalerite surface. Unfortunately, this large polynuclear complex demands a lot of computer time for the ab initio DFT calculations. However, already for the complex analyzed here, it can be inferred that the structure around the Zn atom gives rise to the observed spectral difference in the region 500–650 cm^{-1}.

The intense 970 cm^{-1} band in the infrared spectrum of the Ni compound (Fig. 4 and Table 3) belongs to the modes with considerable P–O stretching content, whilst the other one at 1007 cm^{-1} belongs to the vibrational modes with considerable C–O stretching content. The shoulder at 960 cm^{-1} and the resolved band at 976 cm^{-1} in the infrared spectrum of the Zn compound (Fig. 4 and Table 4) correspond to the 970 cm^{-1} band of the Ni compound. Similarly, the 1011 cm^{-1} band in $Zn(DEDTP)_2$ corresponds to the 1007 cm^{-1} band in $Ni(DEDTP)_2$.

Also in the measured infrared spectra there are clear differences between the two complexes. In the frequency region slightly above 600 cm^{-1}, where P–S stretching vibrations contribute more than 60% to the observed absorption (Tables 3 and 4), the $Zn(DEDTP)_2$ complex exhibited a more complicated spectral pattern. This difference was also assigned to the aforementioned difference in structure around the two metal atoms of the complexes.

The measured and calculated $Ni(DEDTP)_2$ spectra are compared in Fig. 5. It can be seen that the frequencies of the experimental and simulated spectra are in good agreement. However, the simulated intensities differ significantly from the measured ones. The reason can be the difference between the condensed state and the single molecule, the weak model of the intensity calculations, and the level of approximation of the quantum chemical calculation. A similar result was observed also when comparing the spectra of $Zn(DEDTP)_2$ (Fig. 6).

Both infrared and Raman spectra were simulated applying a FWHH of 15 cm^{-1}. The calculated Raman intensities (S_i) for the ith vibrational mode (with ν_i frequency) were corrected to the excitation wavelength (i.e. ν_0 frequency) of the experimental spectrum, according to [24]. The following equation was used:

$$I_i = f\frac{(\nu_0 - \nu_i)^4}{\nu_i\left[1 - \exp\left(-\frac{hc\nu_i}{kT}\right)\right]}S_i$$

where T is the temperature (here 293 K), h is Planck's constant, k is Boltzmann's constant and c is the velocity of light in vacuum. The factor f is an arbitrary constant valid for all vibrational frequencies of the molecule.

The simulated spectra are based on calculated frequency positions without considering molecular interactions, relaxation effects, or conformational dynamics, and were based also on the calculated infrared and Raman activities. Therefore the simulated intensities deviate from the experimental ones. Besides, the simulation with constant FWHH for all fundamental frequencies can cause overlap of some bands and also smaller shifts in comparison to the experimental ones.

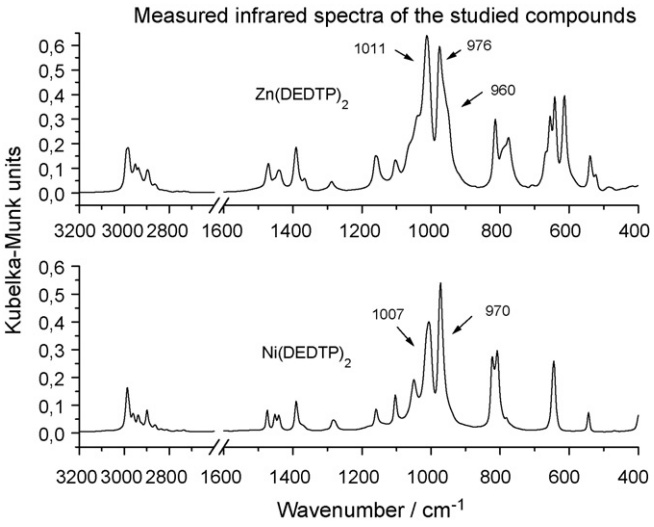

Fig. 4. Measured infrared spectra of the studied compounds.

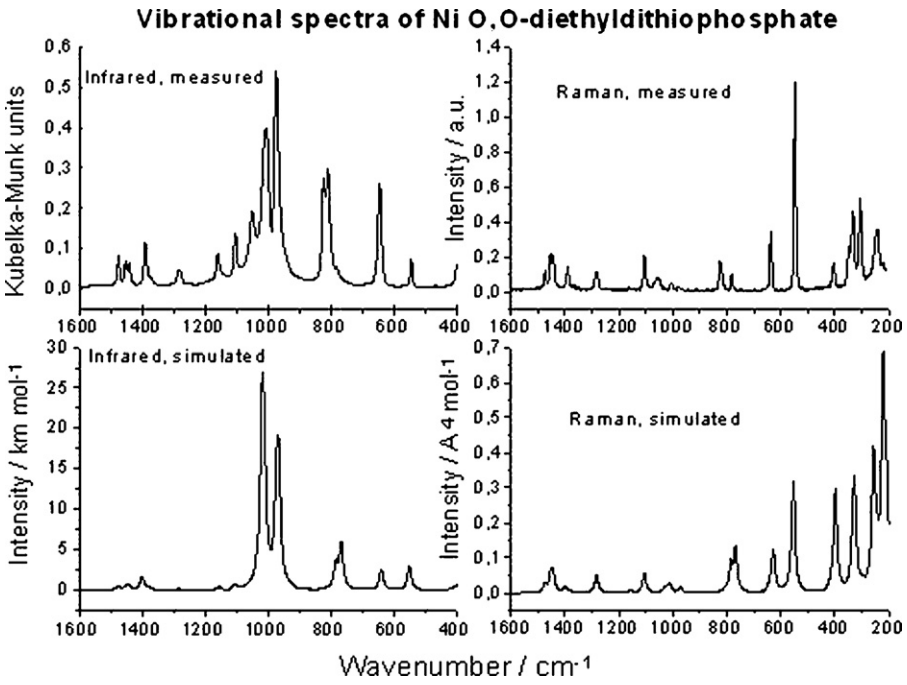

Fig. 5. Vibrational spectra of the nickel complex.

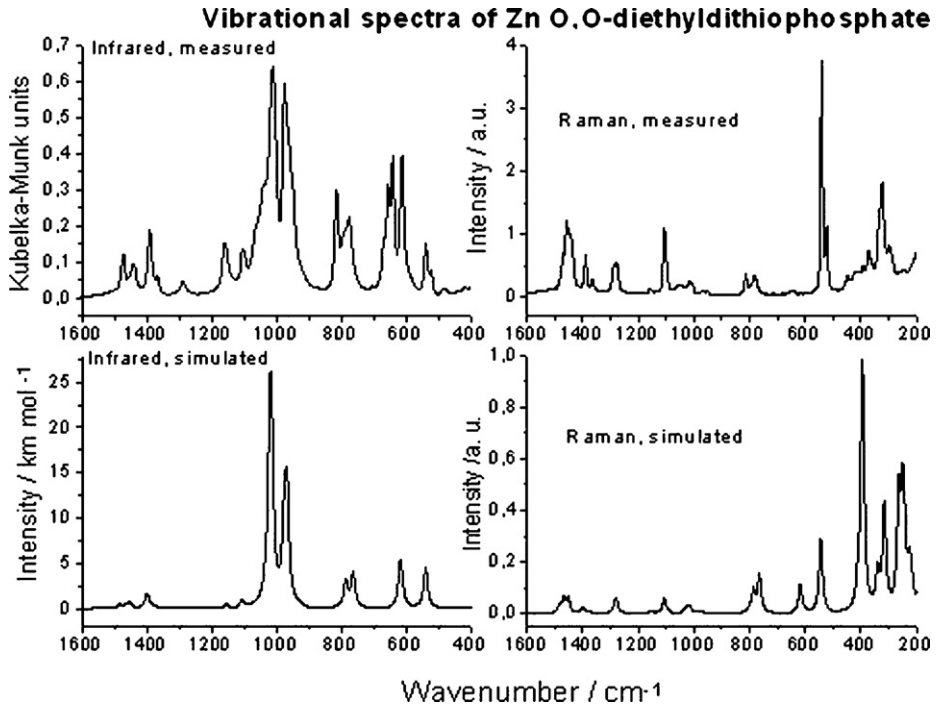

Fig. 6. Vibrational spectra of the Zn complex.

5. Conclusions

Both the investigated formula units were transition metal complexes. The nickel atom formed a dsp^2 hybrid and therefore the PS_2MS_2P entity was planar. The Zn atom, however, formed an sp^3 hybrid, and therefore the S_2ZnS_2 group had tetrahedral like structure (see Section 4.1 and Table 1). The optimized molecular structures support this statement.

There were considerable differences between the $Ni(DEDTP)_2$ and the $Zn(DEDTP)_2$ molecules in the atomic net charges of the PS_2MS S entity both in Mulliken's atomic net charges and in the NBO charges. The P atoms show differences in their Mulliken's atomic net charges but there was practically no difference between the NBO charges of the P atoms (Table 2). The differences between the two metal atoms are reflected very sharply in their atomic net charges. The values for the Zn atom are higher more than 0.5 atomic charge units than those for Ni practically independent of the method.

Regarding the diagonal force constants for the central part, there are not considerable differences in the stretching ones of the two compounds. However, all the deformation force constants introduce large differences.

The vibrational spectra of the two complexes exhibited significant differences in the frequencies belonging to the central part of the formula units i.e. in the frequency region of the PS_2MS_2P entity. Applying DFT calculations it was possible to assign the P–S interaction with the metal atoms to the spectral region between 500 cm^{-1} and 650 cm^{-1}. This knowledge will be valuable in future studies of the interaction between alkylphosphates and metal sulfide or metal–oxide surfaces. The type, i.e. the properties of the metal atom determined the structure of the central entity and therefore the spectral properties of the complex. However, the effect of the metal atom did not extend beyond the phosphorus atoms.

Appendix A. Supplementary data

Supplementary data associated with this article, containing the definition of the internal coordinates, scale factors and vibrational force constants, can be found in the online version, at doi:10.1016/j.vibspec.2010.04.011.

References

[1] S.R. Rao, Surface Chemistry of Froth Flotation, Vol. 2, 2nd edition, Plenum Publishers, New York, 2004.
[2] N.J. Mosey, T.K. Woo, Tribology Int. 39 (2006) 979–993.
[3] M.A. Nicols, T. Do, P.R. Norton, M. Kasrai, G.M. Bancroft, Tribology Int. 38 (2005) 15–39.
[4] K. Hayahashi, Y. Sasaki, S. Tagashira, M. Nakashima, Anal. Sci. 1 (1985) 51–54.
[5] V.K. Chebotarev, Y.K. Kraev, I.V. Voronkina, E.G. Iljina, L.E. Cherdantseva, Talanta 47 (1998) 1043–1051.
[6] S. Jiang, R. Frazier, E.S. Yamaguchi, M. Blanco, S. Dasgupta, Y. Zhou, T. Cagin, Y. Tang, W.A. Goddard, J. Phys. Chem. B 101 (1997) 7702–7709.
[7] J.P. Räsänen, M. Peräklylä, E. Pohjala, T.A. Pakkanen, J. Chem. Soc. Perkin Trans. 2 (1994) 1055–1060.
[8] A. Fredriksson, P. Hellström, S. Öberg, A. Holmgren, J. Phys. Chem. C 111 (2007) 9299–9304.
[9] P. Hällström, A. Holmgren, S. Öberg, J. Phys. Chem. C 111 (2007) 16920–16926.
[10] S. Öberg, A. Fredriksson, A. Holmgren, Spectrochim. Acta A 65 (2006) 887–895.
[11] F. Billes, A. Holmgren, Vib. Spectrosc. 40 (2006) 89–97.
[12] D.B. Barr, R. Bravo, G. Weerasekera, L.M. Caltabiano, R.D. Whitehead Jr., A.O. Olsson, S.P. Caudill, S.E. Schober, J.L. Pirkle, E.J. Sampson, R.J. Jackson, L.L. Needham, Environ. Health Perspect. 112 (2004) 186–200.
[13] R.K. Coswik, R. Srinivasan, J. Chem. Phys. 59 (1973) 5517–5525.
[14] I.M. Oglezneva, V.N. Kirichenko, Zhurnal Strukturnoi Khimii 25 (1984) 164–166.
[15] M.J. Frisch, G.W. Trucks, H.B. Schlegel, G.E. Scuseria, M.A. Robb, J.R. Cheeseman, J.A. Montgomery Jr., T. Vreven, K.N. Kudin, J.C. Burant, J.M. Millam, S.S. Iyengar, J. Tomasi, V. Barone, B. Mennucci, M. Cossi, G. Scalmani, N. Rega, G.A. Petersson, H. Nakatsuji, M. Hada, M. Ehara, K. Toyota, R. Fukuda, J. Hasegawa, M. Ishida, T. Nakajima, Y. Honda, O. Kitao, H. Nakai, M. Klene, X. Li, J.E. Knox, H.P. Hratchian, J.B. Cross, C. Adamo, J. Jaramillo, R. Gomperts, R.E. Stratmann, O. Yazyev, A.J. Austin, R. Cammi, C. Pomelli, J.W. Ochterski, P.Y. Ayala, K. Morokuma, G.A. Voth, P. Salvador, J.J. Dannenberg, V.G. Zakrzewski, S. Dapprich, A.D. Daniels, M.C. Strain, O. Farkas, D.K. Malick, A.D. Rabuck, K. Raghavachari, J.B. Foresman, J.V. Ortiz, Q. Cui, A.G. Baboul, S. Clifford, J. Cioslowski, B.B. Stefanov, G. Liu, A. Liashenko, P. Piskorz, I. Komaromi, R.L. Martin, D.J. Fox, T. Keith, M.A. Al-Laham, C.Y. Peng, A. Nanayakkara, M. Challacombe, P.M.W. Gill, B. Johnson, W. Chen, M.W. Wong, C. Gonzalez, J.A. Pople, Gaussian 03, Revision C. 02, Gaussian, Inc, Wallingford, CT, 2004.
[16] A.D. Becke, Chem. Phys. 98 (1993) 5648.
[17] C. Lee, W. Young, R.G. Parr, Phys. Rev. B 37 (1988) 785–789.
[18] G. Fogarasi, X. You, P.W. Taylor, P. Pulay, J. Am. Chem. Soc. 114 (1992) 8191–8201.
[19] R.S. Mulliken, J. Chem. Phys. 23 (1955) 1833.
[20] A.E. Reed, R.B. Weinstock, F.J. Weinhold, J. Chem. Phys. 83 (1985) 735.
[21] A.E. Reed, F.J. Weinhold, L.A. Curtiss, Chem. Rev. 88 (1988) 899.
[22] A.V. Ivanov, O.N. Antzutkin, A.-C. Larsson, M. Kritikos, W. Forsling, Inorg. Chim. Acta 315 (2001) 26–35.
[23] S.L. Lawton, G.T. Kokotailo, Inorg. Chem. 11 (1969) 2410.
[24] G. Keresztury, S. Holly, G. Besenyei, J. Varga, A. Wang, J.R. Durig, Spectrochim. Acta Part A 49 (1993) 2007–2026.